Guided acoustic waves in layered polymer films: interpretation of Brillouin data

2001 J. Phys.: Condens. Matter 13 7953

(http://iopscience.iop.org/0953-8984/13/35/303)

INSTITUTE OF PHYSICS PUBLISHING JOURNAL OF PHYSICS: CONDENSED MATTER

J. Phys.: Condens. Matter **13** (2001) 7953–7967 PII: S0953-8984(01)22964-6

Guided acoustic waves in layered polymer films: interpretation of Brillouin data

R Hotz, J K Krüger, W Possart and R Tadros-Morgane

Fachbereich Physik, Universität des Saarlandes, D-66041 Saarbrücken, Germany

E-mail: hotz@lusi.uni-sb.de (R Hotz)

Received 16 March 2001, in final form 21 June 2001
Published 16 August 2001
Online at stacks.iop.org/JPhysCM/13/7953

Abstract

We report our theoretical considerations motivated by Brillouin spectra of polymethyl methacrylate (PMMA) films ($d = 13$ nm and $d = 225$ nm) on Si(100) substrates. We have rederived a numerical calculational scheme developed for considering Brillouin experiments on layer systems. It delivers dispersion curves and intensities, indicated here by appropriate hatchings. With backscattering geometry, we observed guided waves in agreement with our calculations. The Brillouin peaks fall on the calculated segments of the dispersion curves visible with the elasto-optic mechanism for 180° scattering or for reflection-induced 'A-scattering' (called RIΘA scattering by Krüger *et al* (Krüger J K, Embs J, Brierley J and Jimenez R 1998 *J. Phys. D: Appl. Phys.* **31** 1913)). The observed pseudo-guided waves for $d = 225$ nm were explained using a model of a PMMA film fixed at one surface and free at the other. For the $d = 225$ nm thick film the Brillouin data provided information on its mechanical constants, but in the $d = 13$ nm case the dispersion curves are not very sensitive to the film properties. The Brillouin data for $d = 13$ nm show the direction of the sagittal plane with respect to the symmetry of the silicon rather than indicating the properties of the PMMA film.

(Some figures in this article are in colour only in the electronic version)

1. Introduction

We used the basic work on elastic wave propagation in thin layers by Farnell and Adler [2]. They solved the equations of linear elasticity theory for plane layers perfectly bound to a substrate half-space: system 'slow on fast' exhibit discrete eigenfrequencies, Ω^j, depending on the component of the wave vector $k_\parallel$ parallel to the layer surface. Segments of the dispersion curves $\Omega^j(k_\parallel)$ can be measured by means of Brillouin light scattering (BLS), and they can give information on the elastic properties of the films [3–6]. Theoretical calculations of the intensities of Brillouin peaks for a layer on a substrate half-space were given by Bortolani

et al [7]. They considered the elasto-optic mechanism as well as the ripple scattering induced by the acoustic phonons. Their theory explained very well concrete Brillouin spectra; see e.g. [8, 9].

In this paper we present Brillouin spectra obtained with p-polarized light, for back-scattering geometry, from PMMA layers ($d = 13$ nm and $d = 225$ nm) on Si(100) substrates [10]. The recorded surface acoustic waves (SAWs) and pseudo-SAWs are the basis for further theoretical considerations. For numerical examples we use the elastic constants and densities of bulk isotropic PMMA and bulk cubic silicon.

First of all, we derive once more a numerical scheme (easy to handle) for calculating dispersion curves and guided modes for a layered film on a substrate. We use transfer matrices as described by Djafari-Rouhani *et al* [11] and in our own work [12–14]. We treat different outer boundary conditions: (I) free-standing films; (II) a film deposited on a substrate half-space; and (III) a film free at one surface and clamped at the other. Asymptotically for growing $k_\parallel d$, their dispersion curves coincide. We discuss the numerical problems that arise and the applicability of the boundary conditions for actual regions of the $(k_\parallel d, \Omega d)$ plane.

With growing layer thickness, the network of dispersion curves becomes denser. To indicate the relevant segments, we show relative intensities by hatchings on the dispersion curves. To explain our experiments it was sufficient to consider the elasto-optic mechanism, even for unknown Pockels constants. For $d \geqslant 1$ μm the calculations show only two small regions in the vicinity of $\Omega/k_\parallel = v_L$ and $\Omega = 2v_L k_I n$ (k_I, n, v_L being the magnitude of the incident light wave vector, the refractive index and the longitudinal sound velocity of PMMA). This result agrees with the experimental observation of RIΘA scattering from PET on silicon (see Krüger *et al* [1]).

We show the sensitivity of the dispersion curves to the substrate, especially to the scattering plane relative to the silicon symmetry, and we show the sensitivity to the constants of PMMA. It turns out that the Brillouin measurements for $d = 13$ nm show the direction of the sagittal plane rather than indicating the elastic properties of the PMMA film. To obtain information on very thin layers, Forrest *et al* [5] experimentally investigated stacks of $(\mathrm{PS/PI})^N$, $N = 1, \ldots, 5$, layers with an overall thickness of $d = 160$ nm. To explain their Brillouin data, they calculated the dispersion curves using an effective-medium theory. To obtain more information, we calculated the dispersion curves exactly for each experiment ($N = 1, 3, 5$) [15, 16].

This paper is organized as follows. Section 2 gives the theory for layered films on a substrate. Section 3 is devoted to the application to PMMA layers on Si(100). Section 4 contains results and a discussion.

2. Theoretical aspects

2.1. The vibrations of a system of N layers

In a system of N layers with thicknesses $d_1, \ldots, d_N$ and plane interfaces, we assume perfect connection of adjacent layers, i.e. the displacements and the normal components of the stress tensor are continuous. Thus a plane sound wave with frequency Ω and wave vector $\vec{k}$ goes through the system with the same sagittal plane (spanned by $\vec{k}$ and the layer normal) and $k_\parallel$ (component of $\vec{k}$ parallel to the layer) in all layers. Therefore for the eigenvibrations of the layered system the *relevant parameters are* $(\Omega, \vec{k}_\parallel)$, i.e. Ω, $k_\parallel$ and the sagittal plane. See figure 1.

In the unbounded ℓth *layer*, the equations of linear elasticity theory lead to plane-wave solutions for the displacements, $\vec{u}_0 \exp(-\mathrm{i}\Omega t + \mathrm{i}\vec{k} \cdot \vec{r})$. There are six waves with the given parameters: sagittal plane, $|k_\parallel|$ and Ω. A linear combination of them with six coefficients

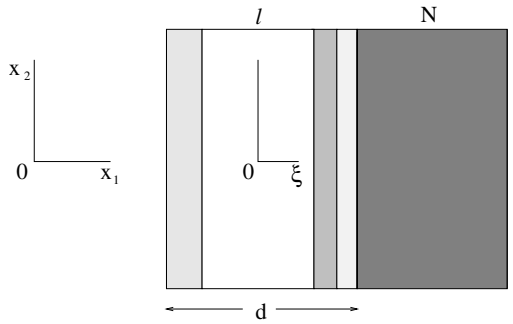

Figure 1. General scenario.

$\vec{A}_\ell = (A_1, \ldots, A_6)^+_\ell$ is the general expression for the vibrations of the layered system[1]:

$$\vec{u}^{(\ell)}(\Omega, \vec{k}_\parallel; \vec{r}, t) = \mathrm{e}^{-\mathrm{i}\Omega t + \mathrm{i}k_2 x_2 + \mathrm{i}k_3 x_3} \mathbf{U}^{(\ell)}(\Omega, \vec{k}_\parallel; \xi)\vec{A}_\ell \tag{1}$$

with $\mathbf{U}^{(\ell)}$ a 3×6 matrix depending on the elastic constants and the density of the layer; ξ is the local coordinate in the x_1-direction with the origin at the middle of the layer. Using Hooke's law, we obtain from equation (1) the three components $\vec{\sigma}_1 = (\sigma_{11}, \sigma_{21}, \sigma_{31})^+$ of the stress tensor normal to the interfaces:

$$\vec{\sigma}_1^{(\ell)}(\Omega, \vec{k}_\parallel; \vec{r}, t) = \mathrm{e}^{-\mathrm{i}\Omega t + \mathrm{i}k_2 x_2 + \mathrm{i}k_3 x_3} \mathbf{S}^{(\ell)}(\Omega, \vec{k}_\parallel; \xi)\vec{A}_\ell \tag{2}$$

with $\mathbf{S}^{(\ell)}$ a corresponding 3×6 matrix. In terms of equations (1) and (2) we obtain the *inner boundary conditions* between the ℓth and $(\ell + 1)$th layers (continuous u_i and σ_{i1}):

$$\mathbf{U}^{(\ell)}(\Omega, \vec{k}_\parallel; d_\ell/2)\vec{A}_\ell = \mathbf{U}^{(\ell+1)}(\Omega, \vec{k}_\parallel; -d_{\ell+1}/2)\vec{A}_{\ell+1} \tag{3}$$

$$\mathbf{S}^{(\ell)}(\Omega, \vec{k}_\parallel; d_\ell/2)\vec{A}_\ell = \mathbf{S}^{(\ell+1)}(\Omega, \vec{k}_\parallel; -d_{\ell+1}/2)\vec{A}_{\ell+1}. \tag{4}$$

We can write this system of equations as

$$\vec{A}_{\ell+1} = \mathbf{M}_{\ell+1,\ell}(\Omega, \vec{k}_\parallel)\vec{A}_\ell. \tag{5}$$

The 6×6 *transfer matrix* $\mathbf{M}_{\ell+1,\ell}$ depends on Ω, $\vec{k}_\parallel$, the densities, the elastic constants and the thicknesses $(d_\ell, d_{\ell+1})$ of both layers. The unknown coefficient vectors of all layers can be derived from $\vec{A}_1$. $\vec{A}_1$ is to be determined according to the boundary conditions at the outer surfaces of the layer system, e.g. *boundary conditions (I): both outer surfaces are free*. In terms of equation (2) they can be written as three equations for $\vec{A}_1$ and three equations for $\vec{A}_N$:

$$\mathbf{S}^{(1)}(\Omega, \vec{k}_\parallel; -d_1/2)\vec{A}_1(\Omega, \vec{k}_\parallel) = 0 \tag{6}$$

$$\mathbf{S}^{(N)}(\Omega, \vec{k}_\parallel; d_N/2)\vec{A}_N(\Omega, \vec{k}_\parallel) = 0. \tag{7}$$

With the transfer matrices of all layers, equation (5), $\vec{A}_N$ may be expressed in terms of $\vec{A}_1$. From equations (6) and (7) we arrive at a system of six equations for the six unknown coefficients $\vec{A}_1$ of the first layer of the system:

$$\mathbf{M}_\mathrm{I}(\Omega, \vec{k}_\parallel)\vec{A}_1(\Omega, \vec{k}_\parallel) = 0. \tag{8}$$

For each sagittal plane and $k_\parallel$ (i.e. $\vec{k}_\parallel$) the eigenvalue equation $\det \mathbf{M}_\mathrm{I}(\Omega, \vec{k}_\parallel) = 0$ gives an infinite number of discrete eigenfrequencies $\Omega_\mathrm{I}^j(\vec{k}_\parallel)$, $j = 1, 2, 3, \ldots$. To calculate the associated normal modes, we introduce the following normalization for layer systems:

$$\sum_{\ell=1}^{N} \rho_\ell \int_{-d_\ell/2}^{d_\ell/2} |\vec{u}^j(\vec{k}_\parallel; \vec{r})|^2 \, \mathrm{d}\xi = 1. \tag{9}$$

[1] $\vec{v}^+$ means the transposed vector.

If we consider the half-space instead of the Nth layer, the corresponding integral runs from 0 to infinity. This integral converges in the region investigated: $\Omega/k_\parallel < v'_{lim}$ (non-propagating modes in the substrate). It can be shown that the normal modes are then mutually orthonormal:

$$\int_V \rho(\vec{r})\vec{u}^j(\vec{k}_\parallel;\vec{r})\cdot\vec{u}^{j'*}(\vec{k}'_\parallel;\vec{r})\,\mathrm{d}V = \delta_{jj'}\delta(\vec{k}_\parallel - \vec{k}'_\parallel). \tag{10}$$

Each vibration of the layered system can be expanded in normal modes:

$$\vec{u}(\vec{r},t) = \sum_j \int Q_j(\vec{k}_\parallel;t)\vec{u}^j(\vec{k}_\parallel;\vec{r})\,\mathrm{d}k_2\,\mathrm{d}k_3. \tag{11}$$

The normal coordinates $Q_j(\vec{k}_\parallel;t)$ are independent harmonic oscillators with the equations of motion $\ddot{Q}_j = -\Omega^{j2}Q_j$. Their quantization leads to the following expression in terms of creation and annihilation oscillator operators:

$$Q_j(\vec{k}_\parallel;t) = \sqrt{\frac{\hbar}{2\Omega^j(\vec{k}_\parallel)}}\left\{a_j(\vec{k}_\parallel)\mathrm{e}^{-\mathrm{i}\Omega^j(\vec{k}_\parallel)t} + a_j^+(\vec{k}_\parallel)\mathrm{e}^{\mathrm{i}\Omega^j(\vec{k}_\parallel)t}\right\}. \tag{12}$$

To calculate the Brillouin intensities (section 2.3), we use the thermal averages

$$\begin{aligned}\langle a_j^+(\vec{k}_\parallel)a_{j'}(\vec{k}'_\parallel)\rangle &= n_j(\vec{k}_\parallel)\delta_{jj'}\delta(\vec{k}_\parallel - \vec{k}'_\parallel)\\ \langle a_j(\vec{k}_\parallel)a_{j'}^+(\vec{k}'_\parallel)\rangle &= (n_j(\vec{k}_\parallel)+1)\delta_{jj'}\delta(\vec{k}_\parallel - \vec{k}'_\parallel)\end{aligned} \tag{13}$$

with the mean occupation number $n_j(\vec{k}_\parallel) = (\mathrm{e}^{\hbar\Omega^j(\vec{k}_\parallel)/k_BT} - 1)^{-1}$.

2.2. Mode polarizations

For composites with isotropic layers, the eigenmodes always can be separated into *p-modes* (they involve only displacements in the sagittal plane; e.g. Rayleigh and Sezawa modes) and *a-modes* (with anti-plane displacements, i.e. polarized vertical to the sagittal plane; e.g. Love modes). Also in our examined system, with cubic Si substrates and isotropic PMMA layers in the sagittal planes (010), (001), (011) the modes decouple into p-modes and a-modes. For p–p polarized light the elasto-optic mechanism shows p-modes (sagittal modes) only: these we consider in this paper.

2.3. Brillouin intensities due to the elasto-optic effect

Brillouin light spectroscopy devices measure the spectral density due to thermally excited phonons [17, 18]:

$$S(\vec{q},\omega) \sim \int_0^\infty \mathrm{e}^{\mathrm{i}(\omega-\omega_\mathrm{I})t}\langle\delta\epsilon^*_{SI}(\vec{q};0),\delta\epsilon_{SI}(\vec{q};t)\rangle\,\mathrm{d}t \tag{14}$$

with the spatial integration over the illuminated volume V of the dielectric constant fluctuations:

$$\delta\epsilon_{SI}(\vec{q},t) \equiv \int_V \vec{e}_S\,\delta\epsilon(\vec{r},t)\vec{e}_I\mathrm{e}^{\mathrm{i}\vec{q}\cdot\vec{r}}\,\mathrm{d}\vec{r} \qquad \vec{q} \equiv \vec{k}'_I - \vec{k}'_S. \tag{15}$$

For p–p polarized light, $\delta\epsilon_{SI} = \delta\epsilon_{33}$, i.e. $\vec{E}$ is vertical with respect to the scattering plane, which is the 1, 2-plane in this paper. The elasto-optic effect in the first approximation is described by the Pockels tensor P_{ij}; e.g. for orthorhombic matter,

$$\delta\epsilon_{SI}(\vec{r};t) = \delta\epsilon_{33}(\vec{r};t) = P_{33}u_{3,3} + P_{13}u_{1,1} + P_{23}u_{2,2}. \tag{16}$$

$\langle\cdots\rangle$ is a time-averaged correlation function. In most theoretical calculations the ensemble-averaged correlation function is considered instead; this means that the systems are assumed

to be ergodic. For one-phonon processes it is convenient to deduce the above correlation function from the ensemble-averaged products of creation and annihilation operators of single modes [19]. From the normal-mode expansion, equation (10), we obtain

$$\delta\epsilon_{33}^{j}(\vec{r};t) = \int \mathrm{d}k_2\ \mathrm{d}k_3\ Q^{j}(\vec{k}_{\parallel};t)\,\delta\epsilon_{33}^{j}(\vec{k}_{\parallel};\vec{r}) \tag{17}$$

where in the ℓth layer the expression $\delta\epsilon_{33}^{j}(\vec{k}_{\parallel};\vec{r})$ is given by

$$\delta\epsilon_{33}^{j}(\vec{k}_{\parallel};\vec{r}) = \mathrm{e}^{\mathrm{i}k_2x_2+\mathrm{i}k_3x_3}\left\{P_{33}^{(\ell)}\,\mathrm{i}k_3\mathbf{U}_3^{(\ell)} + P_{13}^{(\ell)}\mathbf{U}_{1,1}^{(\ell)} + \mathrm{i}k_2P_{23}^{(\ell)}\mathbf{U}_2^{(\ell)}\right\}^{j}\vec{A}_{\ell}^{j} \tag{18}$$

with $\mathbf{U}_i^{(\ell)}$ being the ith row of the 3×6 matrix $\mathbf{U}^{(\ell)}$. Now we calculate $\delta\epsilon_{33}(\vec{q};t)$ from equation (15). If the volume V is sufficiently large in the x_2- and x_3-directions, the x_2-integration gives the δ-function $\delta(k_2-q_{\parallel})$ and the x_3-integration gives $\delta(k_3)$. This means that the integration selects modes with

$$\vec{k}_{\parallel} = \vec{q}_{\parallel} = (0, q_{\parallel}, 0). \tag{19}$$

Therefore we obtain

$$\delta\epsilon_{33}^{j}(\vec{q};t) = Q^{j}(\vec{q}_{\parallel};t)I^{j}(\vec{q}) \tag{20}$$

with the integration over the illuminated volume in the x_1-direction:

$$I^{j}(\vec{q}) = \sum_{\ell=1}^{N}\mathrm{e}^{-\mathrm{i}q_{\perp(\ell)}x_{(\ell)}}\int_{-d_\ell/2}^{d_\ell/2}\mathrm{e}^{-\mathrm{i}q_{\perp(\ell)}\xi}(P_{13}^{(\ell)}\mathbf{U}_{1,1}^{j(\ell)} + \mathrm{i}q_{\parallel}P_{23}^{(\ell)}\mathbf{U}_2^{j(\ell)})\vec{A}_{\ell}^{j}\,\mathrm{d}\xi. \tag{21}$$

Equation (19) and equation (21) show that a-modes are not visible when using p–p scattering, because they have no components in the scattering plane.

Now we are able to calculate $S(\vec{q},\omega)$:

$$\begin{aligned} S(\vec{q},\omega) &\sim \int_0^{\infty}\mathrm{e}^{\mathrm{i}(\omega-\omega_I)t}\,\mathrm{d}t\sum_{j,j'}I^{j}(\vec{q})I^{j'*}(\vec{q})\langle Q^{j*}(\vec{q}_{\parallel};0),\,Q^{j'}(\vec{q}_{\parallel};t)\rangle \\ &= \int_0^{\infty}\mathrm{e}^{\mathrm{i}(\omega-\omega_I)t}\,\mathrm{d}t\sum_{j}|I^{j}(\vec{q})|^2\frac{\hbar}{2\Omega^{j}}\left\{(n_j(q_{\parallel})+1)\mathrm{e}^{-\mathrm{i}\Omega^{j}t} + n_j(q_{\parallel})\mathrm{e}^{\mathrm{i}\Omega^{j}t}\right\}. \end{aligned}$$

Finally we arrive at

$$S(\vec{q},\omega) \sim \sum_{j=1}^{\infty}\left\{(n_j(q_{\parallel})+1)\delta(\omega-\omega_I+\Omega^{j}(q_{\parallel})) + n_j(q_{\parallel})\delta(\omega-\omega_I-\Omega^{j}(q_{\parallel}))\right\}\frac{\hbar|I^{j}(\vec{q})|^2}{2\Omega^{j}(q_{\parallel})}. \tag{22}$$

For room temperature, $n_j \approx n_j + 1 \approx k_BT/\hbar\Omega^{j}$ holds.

2.4. A-scattering and 180° scattering

There are two well known scattering geometries (figure 2) of unreflected light beams in layered films (without birefringence).

- **A-scattering** (e.g. for a free-standing film): the incident angle Θ between $\vec{k}_I$ and the layer normal is the same as the scattered angle Θ. As a result, within each layer of the film the difference $\vec{q} \equiv \vec{k}_I' - \vec{k}_S'$ is parallel to the film:

$$q_{\parallel} = 2k_I\sin\Theta \qquad q_{\perp} = 0. \tag{23}$$

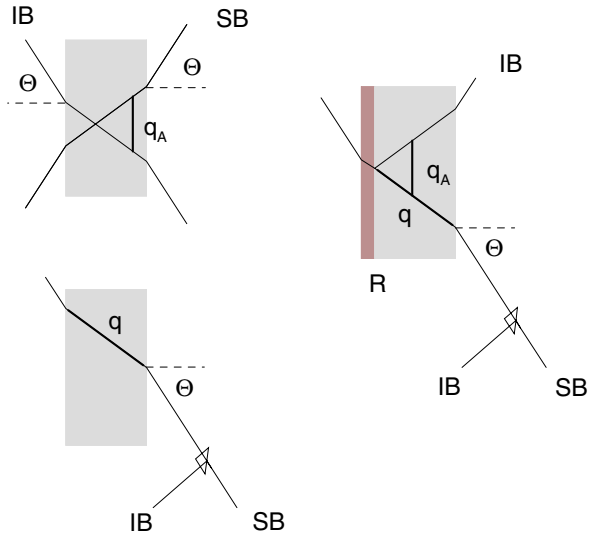

Figure 2. Scattering geometries. IB: incident laser beam; SB: scattered beam; R: reflecting interface. Left: A-scattering and 180° scattering. Right: RIΘA scattering.

- **180° scattering** (e.g. for a film on a substrate): in the layer with the refractive index n, the relevant difference vector $\vec{q} \equiv \vec{k}'_I - \vec{k}'_S = 2\vec{k}'_I$ does not point in the layer direction:

$$q_\parallel = 2k_I \sin\Theta \qquad q_\perp = 2k_I\sqrt{n^2 - \sin^2\Theta}. \tag{24}$$

With backscattering geometry, we observe in the first approximation the direct and one reflected beam at the interface (say the Si surface), i.e. 180° scattering and A-scattering, the latter diminished in intensity. This was described as *RIΘA scattering* for a PET film on silicon by Krüger *et al* [1].

3. PMMA layers on Si(100) substrates

Using Brillouin light spectroscopy in the 180° backscattering geometry, we investigated two samples: PMMA layers of thicknesses $d = 225$ nm and $d = 13$ nm on Si(100) substrates. The angles recorded between the surface normal and incident laser beam were $\Theta = 35°, 40°, 45°$, 50° and 55°. The incident light was polarized with $\vec{E}$ vertical to the scattering plane (defined by its wave vector $\vec{k}_I$ and the surface normal).

To give a concrete example, we continue the numerical analysis with the cubic elastic constants for bulk silicon ($c'_{11} = 166$ GPa, $c'_{12} = 63.9$ GPa, $c'_{44} = 79.6$ GPa, $\rho' = 2.33$ g cm^{-3}) and assumed isotropic elastic constants for bulk PMMA ($c_{11} = 8.54$ GPa, $c_{44} = 2.12$ GPa, $\rho = 1.18$ g cm^{-3}). The latter we derived from our measurements on a thick film ($d > 100\,\mu$m) produced by dip-coating using the same parent material as the thin films were prepared from.

3.1. Regions in the ($k_\parallel d$, Ωd) plane: SAWs and pseudo-SAWs

Propagating plane sound waves $\vec{u}_0 \exp(-\mathrm{i}\Omega t + \mathrm{i}\vec{k}\cdot\vec{r})$ in isotropic PMMA exist only for $\Omega/k_\parallel \geqslant v_T = 1.34$ km s^{-1} (transverse threshold).

The threshold for propagating plane sound waves in cubic Si depends on the sagittal plane and the polarization. For p-modes in the sagittal planes (010) and (001), it is

$v'_{lim}(010) = 5.65$ km s^{-1}, and it is $v'_{lim}(011) = 5.83$ km s^{-1} in the sagittal plane (011). For comparison, $\sqrt{c'_{44}/\rho'} = 5.84$ km s^{-1}.

In the *PMMA region*, $\Omega/k_\parallel \leqslant v'_{lim}$, p-modes are PMMA vibrations decaying into the Si substrate. The composite modes are guided waves in the PMMA layer: surface acoustic waves, *SAWs*.

We call the remaining part of the $(k_\parallel d, \Omega d)$ plane the *Si region*: $\Omega/k_\parallel \geqslant v'_{lim}$, although the modes of the composite consist there of PMMA and Si vibrations. Composite modes with $\Omega/k_\parallel > v'_{lim}$ but with speeds below the longitudinal threshold are called *pseudo-SAWs*. They are partially confined to the PMMA film.

3.2. The outer boundary conditions

- **(I) A free system of two layers: PMMA (thickness d) on Si(100) (thickness d').** For the given sagittal plane and $k_\parallel d$, the eigenvalue equation $\det \mathbf{M}_{\mathrm{I}}(\Omega d, \vec{k}_\parallel d) = 0$ yields an infinite number of discrete eigenfrequencies $\Omega^j_{\mathrm{I}} d$, $j = 1, 2, 3, \ldots$. In the Si region the dispersion curves are very dense—and become even more so as d'/d becomes larger. In the PMMA region, the numerical solution becomes problematic for growing $q_\parallel d$ (see section 4.1). Therefore we consider boundary condition II.
- **(II) A PMMA layer of thickness d on a Si(100) half-space.** For the free PMMA surface, we have the three equations (6) for the PMMA coefficients $\vec{A}_1$. From the boundary condition of limited displacements as $x_1 \to \infty$, we have again three equations for the Si coefficients $\vec{A}_2$. Using the transfer matrix, we write $\vec{A}_2 = \mathbf{M}_{21}\vec{A}_1$, so we arrive at six equations for the six unknown coefficients $\vec{A}_1$:

$$\mathbf{M}_{\mathrm{II}}(\Omega d, \vec{k}_\parallel d)\vec{A}_1(\Omega d, \vec{k}_\parallel d) = 0. \tag{25}$$

  Without numerical problems, the dispersion equation $\det \mathbf{M}_{\mathrm{II}}(\Omega d, \vec{k}_\parallel d) = 0$ leads to discrete dispersion curves $\Omega^j_{\mathrm{II}}(k_\parallel d)$ in the PMMA region ($\Omega/k_\parallel < v'_{lim}$) (see figure 3). In the Si region there is a continuum of eigenfrequencies; i.e. no dispersion curves are defined.
- **(III) A PMMA layer of thickness d with one surface free and the other fixed.** There are, once more, the three equations (6) for the free surface, and also three equations for the clamped surface:

$$\mathbf{S}^{(1)}(\Omega d, \vec{k}_\parallel d; -d/2)\vec{A}_1(\Omega, \vec{k}_\parallel) = 0 \tag{26}$$

$$\mathbf{U}^{(1)}(\Omega d, \vec{k}_\parallel d; d/2)\vec{A}_1(\Omega, \vec{k}_\parallel) = 0 \tag{27}$$

  or, in convenient notation,

$$\mathbf{M}_{\mathrm{III}}(\Omega d, \vec{k}_\parallel d)\vec{A}_1(\Omega d, \vec{k}_\parallel d) = 0. \tag{28}$$

  There are infinitely many discrete dispersion curves $\Omega^j_{\mathrm{III}}(k_\parallel d)$, $j = 1, 2, 3, \ldots$. They are deposited in the Si region and in the PMMA region; see figures 3 and 6, later.

4. Results and discussion

4.1. Dispersion curves

BLS backscattering experiments determine the sagittal plane which is the scattering plane, and it selects

$$k_\parallel = q_\parallel = \frac{4\pi}{\lambda_I} \sin\Theta. \tag{29}$$

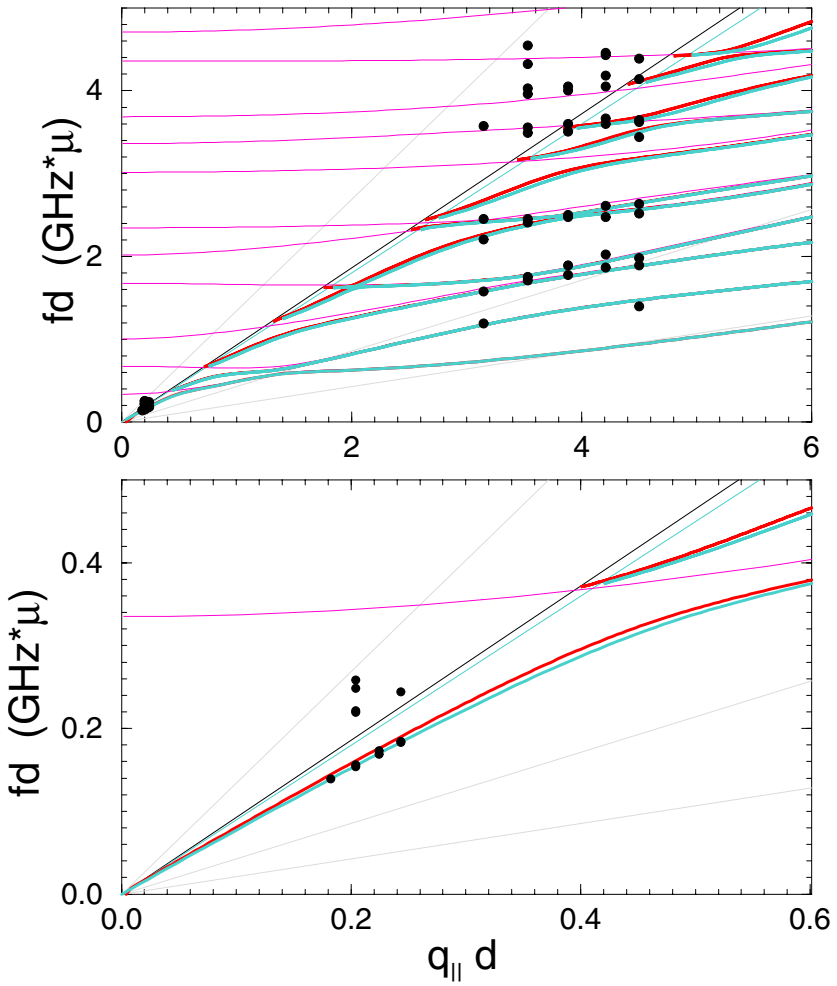

Figure 3. Dispersion curves. (II) a PMMA layer on a Si half-space: thick curves: grey in the scattering plane (001) and black in the plane (011) with respect to the Si symmetry. (III) for a fixed substrate: thin black curves and •: our measured Brillouin peaks for $d = 13$ nm ($q_\parallel d < 0.3$) and $d = 225$ nm ($3 < q_\parallel d < 5$); grey straight line: $2\pi f/q_\parallel = v'_{lim}(001)$; black straight line: $2\pi f/q_\parallel = v'_{lim}(011)$. The top and bottom panels show different sections of the fd versus $q_\parallel d$ plot.

The condition $\det \mathbf{M}(q_\parallel d, \Omega d) = 0$ (from equation (8), (25) or (28)) yields the dispersion curves $\Omega^j(q_\parallel d)$ with $\Omega = 2\pi f$. Different sections of the same plot of the dispersion curves, fd versus $q_\parallel d$ (figure 3), represent the experiments on different samples: $d = 13$ nm ($q_\parallel d \approx 0.18$–$0.24$), $d = 225$ nm ($q_\parallel d \approx 3.2$–$4.5$) and e.g. $d = 900$ nm ($q_\parallel d \approx 13$–18).

Numerical problems arise with the boundary condition (I): a free double layer: PMMA (d) on Si(100) (d') for large d'/d. In the *Si region*, $\Omega/q_\parallel > v'_{lim}$, the set of dispersion curves, $\Omega_{\mathrm{I}}^j(q_\parallel d)$, becomes denser as d'/d grows and the calculation needs more time. The value of d'/d is limited due to the resolving power of the computer. $d'/d \to \infty$ leads to the boundary condition (II) with a continuous spectrum (no discrete dispersion curves). In the *PMMA region*, $\Omega/q_\parallel < v'_{lim}$, the set of dispersion curves Ω_{I}^j is nearly independent of d'/d. But the calculation

of the dispersion curves and modes is limited to small $q_\parallel d$. For example, if $d'/d = 10$ the dispersion curves $j = 1, 2, 3, 4$ can still be calculated for $q_\parallel d = 5$, but the accuracy is no longer sufficient for the modes. See the irregular hatching in figure 6, later. The reason for this is the gigantic magnitude of $\det \mathbf{M}_\mathrm{I}(q_\parallel d, \Omega d)$ for $(q_\parallel d, \Omega d)$ between the dispersion curves, due to the Si partial waves. The boundary condition (II) avoids these exponentially growing terms.

For investigations of SAWs ($\Omega/q_\parallel < v'_{lim}$) the relevant boundary condition is (II); see figures 3, 4, 5. The dispersion equation can be solved for the whole region without numerical problems. The dispersion curves $\Omega^j_\mathrm{II}(q_\parallel d)$ are nearly the same as the curves $\Omega^j_\mathrm{I}(q_\parallel d)$. For $d' = 10d$, visible differences are already limited to $q_\parallel d < 0.7$. With growing PMMA layer thickness d, the boundary conditions become unimportant. Asymptotically as $q_\parallel d \to \infty$, the dispersion curves for the boundary conditions (I), (II) and (III) coincide for each j:

$$\Omega^j_\mathrm{I}(q_\parallel d) \sim \Omega^j_\mathrm{II}(q_\parallel d) \sim \Omega^j_\mathrm{III}(q_\parallel d) \qquad j = 1, 2, 3, \ldots. \tag{30}$$

The number of dispersion curves grows linearly with $q_\parallel d$. Calculation of intensities becomes necessary to mark the relevant segments.

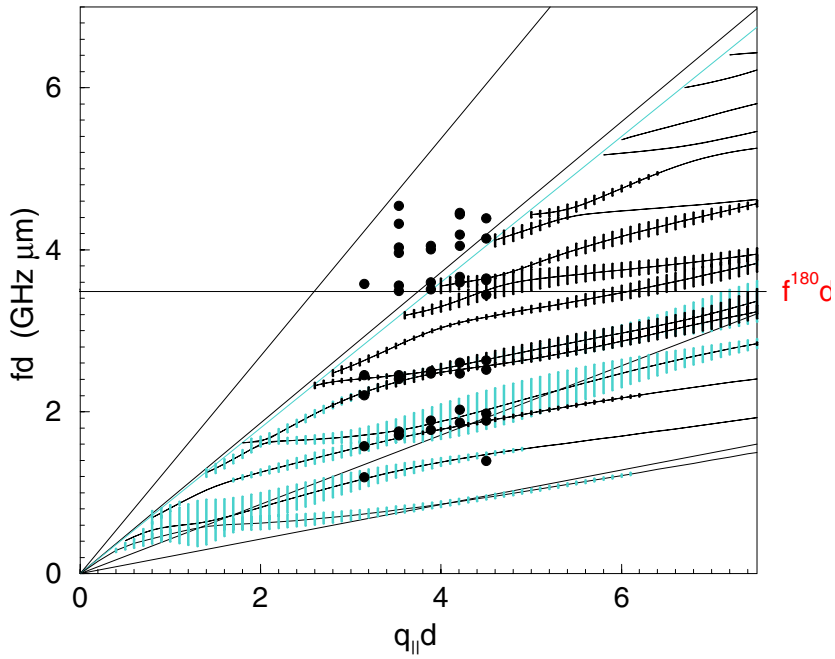

Figure 4. Dispersion curves and Brillouin intensities for (II): a PMMA layer on a Si(100) half-space, with scattering plane (001). •: our measured Brillouin peaks for $d = 225$ nm; A-intensities: grey hatching; 180° intensities for $d = 225$ nm: black hatching; straight lines: $(2\pi f/q_\parallel)^2 = c_{44}/\rho$, c_{11}/ρ, c'_{44}/ρ', c'_{11}/ρ' and $2\pi f/q_\parallel = v'_{lim}(001)$.

In isotropic systems the dispersion curves $\Omega^j_\mathrm{II}(q_\parallel d)$ are the same for each sagittal plane containing the layer normal, but with cubic silicon this is not the case. Numerically, we consider the scattering planes (011) and (001) with respect to the silicon symmetry. (010) has the same properties as (001). In these planes the modes disintegrate into shear horizontal and sagittal modes. And we consider only sagittal modes, since only these are visible with p–p backscattering. In the vicinity of the limiting line $\Omega/q_\parallel = v'_{lim}$, the (011) and (001) curves clearly differ; see figure 3. But at some distance away ($\Omega/q_\parallel < 0.8v'_{lim}$), one can neglect the difference. Than one may even regard the substrate as isotropic; see figure 5.

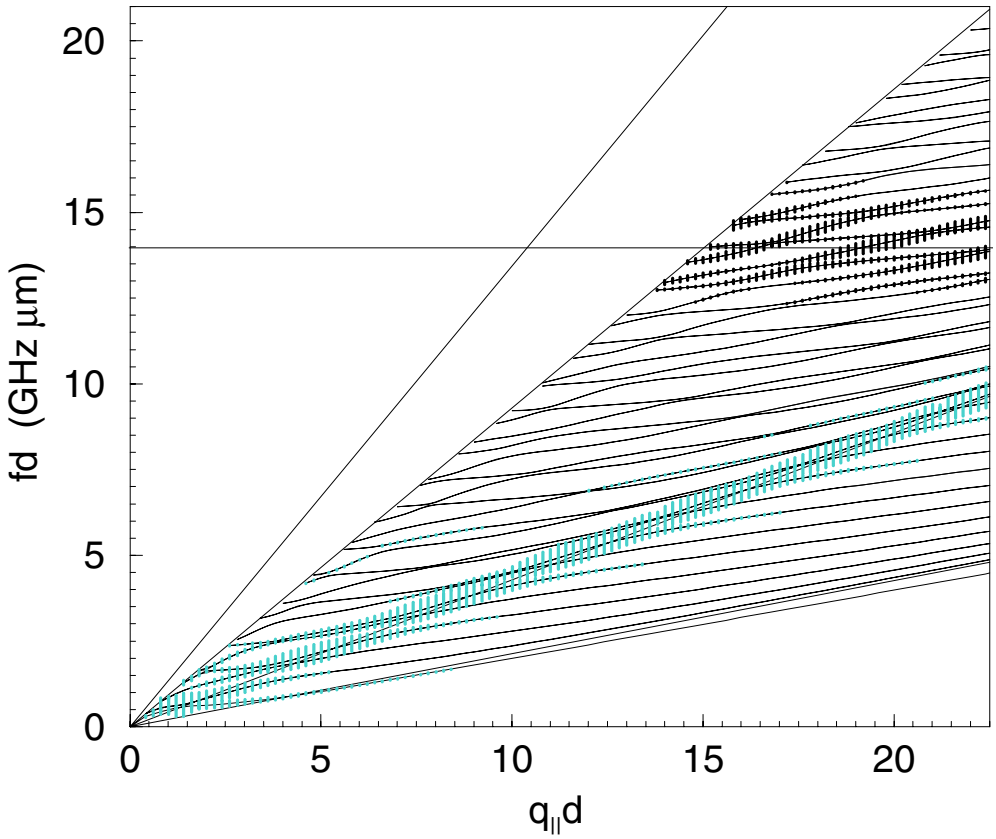

Figure 5. Dispersion curves and Brillouin intensities for (II): a PMMA layer on a Si half-space. The calculation was with an isotropic substrate ($c'_{11}, c'_{44}, c'_{12} = c'_{11} - 2c'_{44}$). A-intensities: grey hatching; 180° intensities for $d = 900$ nm: black hatching; straight lines: $(2\pi f/q_\parallel)^2 = c_{44}/\rho$, $c_{11}/\rho, c'_{44}/\rho', c'_{11}/\rho'$.

With the boundary conditions (II) we obtain dispersion curves only in the PMMA region. To get insight into the Si region, e.g. for pseudo-SAWs, we calculated dispersion curves with the boundary condition (III); see figures 3 and 6. The dispersion curves $\Omega^j_{\mathrm{III}}(q_\parallel d)$ explain the pseudo-SAWs of the $d = 225$ nm sample. Also, the boundary conditions (I), figure 6, test the Si region. For $d' \gg d$, the dispersion curves densely cover the region and deliver no information. We need the intensities.

4.2. Intensities due to the elasto-optic effect

At each point of the dispersion curves we calculate the coefficients $\vec{A}_1$ and, with the transfer matrix, also $\vec{A}_2$. The displacements are given by equation (1). Normalized using equation (9), they yield the normal modes.

The intensity in equation (22) should be calculated from the integration, equation (21): the factor $\exp(-\mathrm{i}q_\perp\xi)$ under the integral is 1 for A-scattering. For 180° scattering it depends on the refractive indices of the layers; see equation (24). For cubic matter, $P_{23} = P_{13}$ holds; thus we have to consider only one Pockels constant for each layer. For guided modes the depth of penetration into the substrate is small. Therefore we expect only a small contribution from the

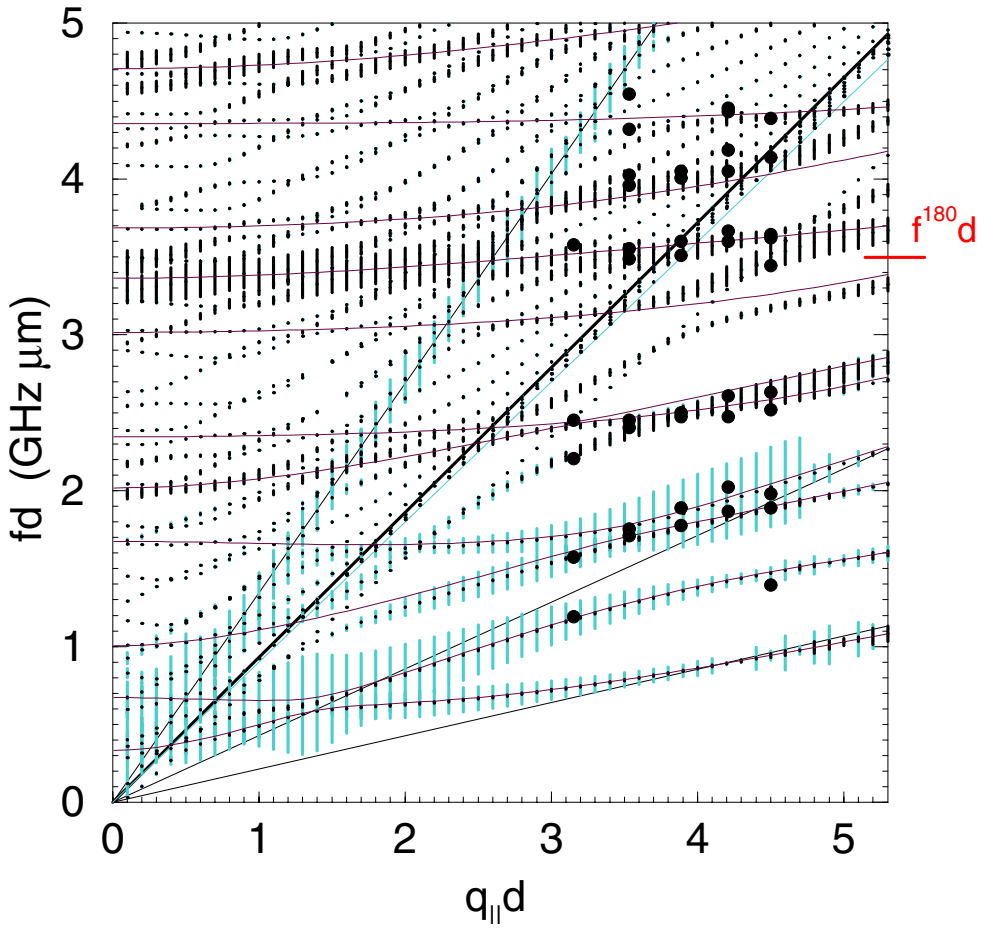

Figure 6. (I) A PMMA layer ($d = 225$ nm) on a Si(100) layer ($d' = 10d$). The scattering plane is (001) with respect to the Si symmetry. •: our measured Brillouin peaks; A-intensities: grey hatching; 180° intensities: black hatching; black curves: dispersion curves (III) for a fixed substrate; straight lines: $(2\pi f/q_\parallel)^2 = c_{44}/\rho, c_{11}/\rho, c'_{44}/\rho', c'_{11}/\rho'$ and $2\pi f/q_\parallel = v'_{lim}(001)$.

substrate, such that the constant P'_{13} (for the substrate) becomes less important. Nevertheless, we calculate the intensities with $P'_{13} = P_{13} = 1$ and $P'_{13} = 0, P_{13} = 1$ for comparison. We calculate A-intensities and 180° intensities separately (thought they could interfere) and show them with an appropriate overall factor as hatching (bars of length $\sim |J^j|^2/\Omega^2$) along the dispersion curves. Figures 4–6 show the results with $P'_{13} = P_{13} = 1$. With $P'_{13} = 0$, $P_{13} = 1$ we obtain nearly the same results as in figures 4 and 5. In the vicinity of the $d = 225$ nm measurements, the difference is generally much less then 10%.

A-intensities ($q_\perp = 0$) depend only on $q_\parallel d$. They can be illustrated in one plot for samples with different layer thicknesses (grey hatching in figures 4, 5 and 6). They show the predominantly longitudinal modes. The visible segments of the dispersion curves lie in a region around the straight line $\Omega/q_\parallel = v_L$(PMMA). This region decreases with $q_\parallel d$. For $q_\parallel d = 18$ (e.g. for $\Theta = 55°$, $d = 900$ nm) there are about 40 dispersion curves, but only one shows marked intensity.

180° intensities ($q_\perp \neq 0$) depend on $q_\parallel d$ and on $q_{\perp(\ell)} d$. For backscattering geometry, in

the ℓth layer, the difference vector, $\vec{q} = \vec{k}'_I - \vec{k}'_S = 2\vec{k}'_I$, has the magnitude $q = 2n_\ell k_I$, where n_ℓ is the refractive index of the layer. Therefore we have

$$q_{\perp(\ell)} = \sqrt{(2n_\ell k_I)^2 - (q_\parallel)^2} \qquad \text{for } q_\parallel < 2n_\ell k_I. \tag{31}$$

We then exactly solve the integral, equation (21). In figures 4, 5 and 6 the resulting 180° intensity is shown as black hatching.

To obtain an estimate of where the 180° intensities are localized in the fd versus $q_\parallel d$ plot, we discuss sufficiently thick layers. For p–p polarized light, a Brillouin peak appears from the longitudinal sound waves of the ℓth layer at $\Omega = q v_L(\ell)$. Therefore we expect for our examples a maximum of intensity in a region around

$$f^{180} = v_L \, 2n_1/\lambda_I. \tag{32}$$

The exact numerical calculations confirm this estimate. The plot of the dispersion curves (fd versus $q_\parallel d$) shows different active horizontal stripes for PMMA layers with different thicknesses d (see figures 4 and 5). In these examples the widths of the stripes Δfd are approximately 2 GHz μm. The active frequency interval Δf therefore becomes smaller, as $1/d$, for thicker PMMA layers.

4.3. Pseudo-SAWs

For $v'_T < \Omega/q_\parallel < v'_L$ the modes are guided only partially; their transverse partial waves lose energy into the substrate. To get insight into this region, we consider the boundary condition (I): a PMMA layer of thickness d on a Si(100) layer of thickness d'. In figure 6 we mark the calculated points of the dispersion curves for $d' = 10d$. The hatching (vertical bars) is proportional to the intensities calculated with equation (22). If we enlarge the thickness d'/d of the substrate, the set of dispersion curves becomes denser. The *A-intensities* (grey hatching) grow. They are located near the $\Omega/q_\parallel = v'_L$ line: they come from the longitudinal partial waves of the substrate. But the pattern of *180° intensities* for $d = 225$ nm (black hatching) does not really change with growing d'/d. It appears in the vicinity of the observed pseudo-SAWs of the sample with $d = 225$ nm. The relative intensity of the pattern is weak for the highest frequencies, but there the measured Brillouin intensities are weak too. We have shown all of our measured Brillouin peaks as black bullets of the same size, even if their relative intensity was very weak (e.g. for $q_\parallel d = 3.53$: $fd = 4.32, 4.54$ GHz μm; and for $q_\parallel d = 4.21$: $fd = 4.43, 4.45$ GHz μm).

Another explanation of the measured pseudo-SAWs for the $d = 225$ nm sample comes from the dispersion curves with the boundary condition (III), the continuous black curves in figure 6. Their neighbourhood of the measurements shows that the pseudo-SAWs for $d = 225$ nm are predominantly PMMA vibrations, while the substrate is scarcely involved.

For two of the four experiments with the $d = 13$ nm sample, we observed weak pseudo-SAWs too. They are located well below the dispersion curves (III); see figure 3. They cannot be explained in terms of the elasto-optic effect on sagittal modes.

4.4. Very thin PMMA films ($d < 15$ nm)

The measured Brillouin peaks lie accurately on one line—the dispersion curve of the scattering plane (001) with respect to the Si symmetry; see figure 3. (010) has the same properties. But the dispersion curve of the scattering plane (011) is clearly different.

We also examined the sensitivity of the dispersion curves to the elastic constants and ρ for the layer. As an example we show in figure 7 three sets of dispersion curves due to the

sagittal plane (001). The constants were from section 3, and moreover $C_{44} \pm 40\%$. One can see that the sensitivity is generally not sufficient for determining elastic constants for very thin single ad-layers ($d < 15$ nm). An important task is to study *very thin* layers, e.g. to test the assumed changes of the elastic properties, when the layers become smaller. Forrest *et al* [5] treated this problem in investigating layer systems. Their Brillouin measurements on stacks of $(PS/PI)^N$ layers with an overall thickness $d = 160$ nm ($N = 1, 3, 5$) are very interesting. But their data analysis, based on an effective-medium theory, can be improved, by performing exact calculations for the different layer systems on silicon [15, 16].

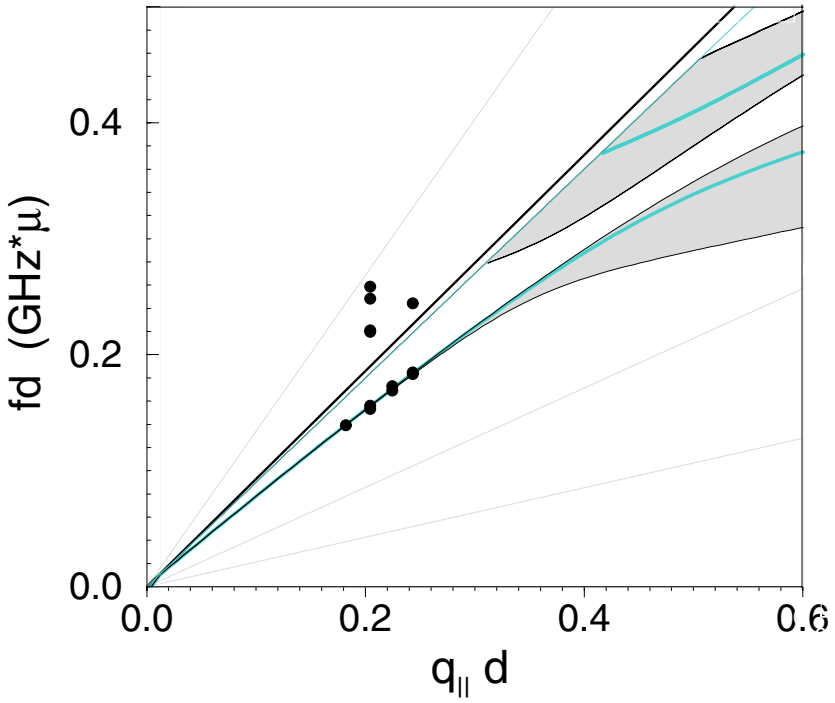

Figure 7. The sensitivity of the dispersion curves to c_{44}; boundary condition (II) for the (001) sagittal plane relative to the Si symmetry; thick grey curves: for $c_{44} = 2.12$ GPa; thin black curves: for $c_{44} \pm 40\%$; •: our measured Brillouin peaks for the sample with $d = 13$ nm.

5. Conclusions

The theory of surface BLS on layered systems has been under development for a long time. Single Brillouin spectra are completely explained and the elastic properties of ad-layers have been determined in many cases. Questions remain concerning the changes of elastic properties for different boundary conditions of very thin layers as compared to the bulk. Inter-layer and adhesion problems that arise are still an active field of research.

Motivated by our BLS experiments for PMMA layers ($d = 13$ nm, $d = 225$ nm) on silicon, we rederived a numerical calculational scheme including boundary conditions ((I), (II), (III)). Therein, we investigated unusual aspects in order to get an overview. This could help with planning of further experiments.

In the fd versus $q_\parallel d$ plane we found different regions of sensitivity to the layer properties, the substrate and the boundary conditions. For example, in the vicinity of $\Omega/q_\parallel = v'_{lim}$ the

dispersion curves are sensitive to the substrate and the boundary conditions. One can clearly distinguish different scattering planes relative to the symmetry of the substrate. But it is impossible to get precise information on the elastic properties of very thin *single* ad-layers ($d < 15$ nm).

For every point of the dispersion curves, we calculated the sagittal modes, the 180° intensities and reflection-induced A-intensities due to the elasto-optic effect. We show these intensities for a large area of the set of dispersion curves as bars (hatching) of proportional length. We have not yet considered the ripple intensities. Their amplitudes are proportional to the shear components of the sagittal modes. As a film gets thicker the increasingly dominant contribution is from the elasto-optical response of the film [7, 21]. In the end, for concrete experiments, the interference of all contributions must be taken into account.

We were able to explain our $d = 225$ nm experiment completely, including the pseudo-SAWS. Also, the guided waves for $d = 13$ nm lie accurately on the calculated dispersion curve for the scattering plane (001) in relation to the silicon symmetry. But the weak pseudo-SAWs seem not to be due to the elasto-optic response of the sagittal modes.

In figure 5 our calculations for a virtual experiment with $d = 900$ nm show a visible region around $2\pi f^A/q_\parallel = v_{L(\mathrm{PMMA})}$ (A-scattering). Additionally this figure shows a small visible horizontal stripe (180° scattering) around $f^{180} = 2v_{L(\mathrm{PMMA})}n_{(\mathrm{PMMA})}/\lambda_I$. This explains the scattering mechanisms investigated and the crossover to thicker ad-layers, where RIΘA scattering was observed [1].

The investigation of pseudo-SAWs using boundary condition (I) to calculate intensities is also new here. It completes the Green's function method used by Akjouj *et al* [20]. The density of states shows resonances in the substrate region $\Omega/q_\parallel > v'_T$, such that they could extend the dispersion curves for guided waves into this region. Akjouj *et al* found, very close to these curves for an Al layer on W (except the first two), the dispersion curves of an Al slab having one surface free and the other rigidly bound (due to the large difference between the elastic constants of W and Al). This corresponds to our observation that the measured pseudo-SAWs of the $d = 225$ nm PMMA layer on Si are described by the boundary condition (III). The advantage of our approach concerns the Brillouin intensities, which match the relevant segments of the dispersion curves. Also, we incorporated the cubic anisotropy of the substrate. Finally, we were able to confirm our calculations by means of experiments.

Acknowledgments

This work was supported by the Deutsche Forschungsgemeinschaft. One of us (RH) gratefully acknowledges discussion with Professor Dr Manfred Lücke.

References

[1] Krüger J K, Embs J, Brierley J and Jimenez R 1998 *J. Phys. D: Appl. Phys.* **31** 1913
[2] Farnell G W and Adler E L 1972 *Physical Acoustics* vol 9, ed W P Mason and R N Thurston (New York: Academic)
[3] Hillebrands B, Krams P, Spörl K and Weller D 1991 *J. Appl. Phys.* **69** 938
[4] Mendik M, Ospelt M, Schwarz C, von Känel H and Wachter P 1992 *Phonon Scattering in Condensed Matter* vol 7, ed M Meissner and R O Pohl (Berlin: Springer)
[5] Forrest J A, Rowat A C, Dalnoki-Veress K, Stevens J R and Dutcher J R 1996 *J. Polym. Sci.* B **34** 3009
[6] Wittkowski T, Jorzick J, Jung K and Hillebrands B 1999 *Thin Solid Films* **353** 137
[7] Bortolani V, Marvin A M, Nizzoli F and Santoro G 1983 *J. Phys. C: Solid State Phys.* **16** 1757
[8] Bortolani V, Nizzoli F, Santoro G and Sandercock J R 1982 *Phys. Rev.* B **25** 3442
[9] Nizzoli F, Byloos C, Giovannini L, Botani C E, Ghislotti G and Mutti P 1994 *Phys. Rev.* B **50** 2027

[10] Krüger J K, Possart W, Hotz R and Siems R 1998 *EURADH Conf. (6–11 September)*
[11] Djafari-Rouhani B, Dobrzynski L, Hardouin Duparc O, Camley R E and Maradudin A A 1983 *Phys. Rev.* B **28** 1711
[12] Hotz R, Krüger J K and Siems R 1983 *Solid State Commun.* **46** 155
[13] Hotz R 1988 *PD Dissertation* University of Saarbrücken
[14] Anders S 1993 *Diplomarbeit* Ulm University
[15] Hotz R, Krüger J K and Possart W 2000 *'Physikalische Akustik' DEGA Workshop*
[16] Hotz R and Krüger J K 2001 to be published
[17] Unruh G 1980/81 *Vorlesung: Spektroskopische Methoden der Festkörperphysik*
[18] Berne B and Pecora R 1976 *Dynamic Light Scattering* (New York: Wiley)
[19] Maradudin A A, Montroll E W and Weiss G H 1963 *Theory of Lattice Dynamics in the Harmonic Approximation* (New York: Academic)
[20] Akjouj A, El Boudouti E H, Djafari-Rouhani B and Dobrzynski L 1994 *J. Phys.: Condens. Matter* **6** 1089
[21] Rowell N L and Stegeman G I 1982 *Can. J. Phys.* **60** 1804